Article | Received 24 October 2025; Revised 18 December 2025; Accepted 6 January 2026; Published 12 January 2026
https://doi.org/10.55092/bm20260001

Design and synthesis of Zr-IR825 nanoparticles for photothermal therapy of tumor cells

Yuzi Huang[1,†], Ge Fang[2,†], Wei Wang[1], Shuzhang Xiao[1,*], Qiancheng Jin[1], Wenquan Huang[2,*] and Peng Geng[1,2,*]

[1] Key Laboratory of Inorganic Nonmetallic Crystalline and Energy Conversion Materials, College of Materials and Chemical Engineering, China Three Gorges University, Yichang 443002, China
[2] College of Medicine and Health Science, China Three Gorges University, Yichang 443002, China

† These authors contributed equally to this work.

* Correspondence authors; E-mails: shuzhangxiao@ctgu.edu.cn (S.X.); huangwenquan@ctgu.edu.cn (W.H.); gengpeng@ctgu.edu.cn (P.G.).

Highlights:

- Zr-IR825 nanoparticles were synthesized by self-assembling IR825 with Zr^{4+} ion through a mild sonication route.
- Zr-IR825 nanoparticles exhibited strong NIR light absorption and high photothermal conversion efficiency.
- Zr-IR825 nanoparticles had excellent biological safety.

Abstract: Organic small-molecule near-infrared (NIR) phthalocyanine-based photothermal agents have shown great potential in tumor photothermal therapy. However, their poor water solubility and rapid *in vivo* metabolism pose significant challenges, severely affecting their pharmacokinetic properties and therapeutic efficacy. To overcome these limitations, nanomedicine provides an effective solution. In this study, zirconium ions (Zr^{4+}) were used to coordinate with the carboxyl groups of the IR825 dye molecules, resulting in the successful self-assembly of Zr-IR825 nanoparticles with an average size of approximately 200 nm. These nanoparticles exhibit strong NIR light absorption and high photothermal conversion efficiency (35.7%), while maintaining excellent stability over multiple photothermal cycles, demonstrating their potential as durable photothermal agents. *In vitro* experiments show that Zr-IR825 nanoparticles can effectively kill mouse breast cancer cells under NIR laser irradiation, with negligible dark toxicity. Hemolysis tests further confirm their excellent blood compatibility (hemolysis rate < 5%), meeting biological safety requirements. This study not only developed an efficient Zr-IR825 photothermal nanoparticle but also provided valuable insights for constructing novel NIR phthalocyanine photothermal agents based on the metal-ligand self-assembly strategy. More importantly, compared to the traditional two-step loading method of "organic photothermal agents—nano carriers", this work directly used the photothermal agent IR825 itself as the building unit, rather than as a loaded

Copyright©2026 by the authors. Published by ELSP. This work is licensed under Creative Commons Attribution 4.0 International License, which permits unrestricted use, distribution, and reproduction in any medium provided the original work is properly cited.

guest, coordinating with Zr^{4+} to form stable nanoparticles in one step, demonstrating a minimalist "integrated" material design.

Keywords: phthalocyanine dye; Zr-IR825 nanoparticles; NIR light; photothermal therapy; tumor cells

1. Introduction

Cancer is one of the leading threats to human health, and developing efficient and low-toxicity treatment strategies remains a major challenge in biomedical research [1–3]. Photothermal therapy (PTT), an emerging method for tumor treatment, NIR light to activate photothermal agents, generating localized heat to selectively destroy tumor cells [4,5]. This technique offers several advantages, including non-invasiveness, spatial controllability, and minimal systemic side effects, which have attracted widespread attention [6,7]. To date, researchers had developed a variety of photothermal agents, including organic photothermal agents (e.g., Indocyanine Green (ICG) and IR825), inorganic photothermal agents (e.g., gold nanorods and CuS), and carbon-based nanomaterials (e.g., carbon nanotubes and graphene), and so on [8–11]. Among these photothermal agents, organic small-molecule NIR phthalocyanine dyes had shown considerable potential due to their strong NIR absorption and good biocompatibility [12,13]. However, these molecules typically suffer from poor water solubility, rapid *in vivo* clearance, and undesirable pharmacokinetic behaviors, which severely limit their clinical translation potential [14,15].

To address these challenges, nanomedicine has demonstrated significant value [16–20]. By coordinating small molecule dyes with metal ions to form self-assembled nanoparticles, not only can their solubility and stability be significantly improved, but their accumulation at tumor sites can also be enhanced, thereby boosting therapeutic efficacy [21–26]. Among various metals, zirconium (Zr), as a biocompatible essential trace element, exhibits lower biological toxicity compared to some transition metals (such as copper and iron), making it a promising candidate in biomaterial applications [27–30].

Based on this, this study designed and synthesized a nanometer-scale Zr-IR825 coordination complex. By utilizing the coordination between Zr^{4+} and the carboxyl groups of the IR825 molecules, a stable nanostructure was formed to achieve efficient photothermal therapy (Figure 1). This material not only retains the original photothermal properties of IR825 but also further improves its biocompatibility and stability. Experimental results show that the hemolysis rate of Zr-IR825 nanoparticles is below 5%, indicating excellent blood compatibility. Under NIR laser irradiation, these nanoparticles enable efficient and controllable photothermal conversion, making them suitable for tumor cell ablation. This study provides a new approach for the development of high-performance, biocompatible phthalocyanine-based photothermal agents and holds great significance for advancing the clinical application of precise PTT.

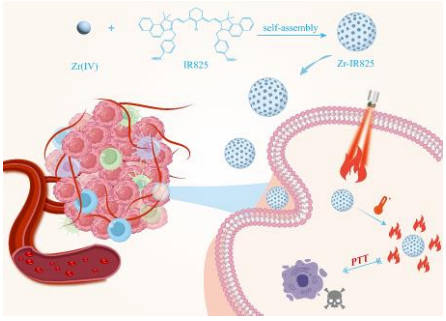

Figure 1. Schematic illustration of the preparation of Zr-IR825 nanoparticles and their PTT application.

2. Methods

2.1. Synthesis of Zr-IR825 nanoparticles

Zr-IR825 nanoparticles were synthesized via a coordination self-assembly method between Zr^{4+} and IR825 molecules. The procedure is as follows: First, 5.0 mg of IR825 was accurately weighed and dissolved in a mixed solution of 20 mL methanol and 0.5 mL triethylamine (volume ratio 39:1). The mixture was stirred magnetically in the dark for 30 min. Then, a methanol/*N, N*-dimethylformamide (DMF) mixed solution (20 mL, with a methanol to DMF volume ratio of 17:3) containing 100.0 mg of $ZrOCl_2 \cdot 8H_2O$ and 50.0 mg of polyvinylpyrrolidone (PVP) was slowly added to the solution. The mixed solution was subjected to ultrasonic treatment in an ultrasonic cleaner (40 kHz) for 6 h, in the dark. Afterward, the solution was transferred to a magnetic stirrer and stirred overnight at room temperature. After the reaction, the final product was collected by centrifugation (10,000 rpm, 5 min) and washed three times each with ethanol and ultrapure water to obtain the Zr-IR825 nanoparticles.

2.2. Photothermal effect testing

To evaluate the photothermal conversion efficiency (PCE) of Zr-IR825 nanoparticles, the sample was dispersed in deionized water to prepare a solution with a concentration of 0.3 mg/mL. A 200 μL aliquot of this solution was placed in a plastic tube and irradiated with an 808 nm NIR laser (power density: 0.8 W/cm^2). The temperature change of the solution was recorded in real-time using a thermographic camera. The PCE was then calculated using the photothermal heating-cooling curves obtained, along with the appropriate formula.

2.3. In vitro photothermal therapy

Under standard conditions, mouse breast cancer (4T1) cells were cultured in DMEM medium containing amino acids and glucose. The cells were seeded into a 96-well plate, and after 24 h, the original medium was replaced with fresh medium containing Zr-IR825 nanoparticles (100 μg/mL). After 6 h of incubation, the cells were irradiated with an NIR laser (808 nm, 1.5 W/cm^2) for different durations (2–8 min) or with different laser powers (0.5–2 W/cm^2) for 8 min. Finally, cell viability under different treatment conditions was assessed using the standard CCK-8 assay.

2.4. Hemolysis experiment

Blood was collected from BALB/c mice (fibrinogen was removed) and washed several times with PBS. A 2% (V/V) RBC solution was prepared by dilution. Different concentrations of Zr-IR825 nanoparticles in PBS were mixed with an equal volume of the RBC solution and left to stand for 4 hours. Deionized water and PBS were used as positive and negative controls, respectively. After high-speed centrifugation, the supernatant was photographed under a microscope, and the absorbance at 541 nm was measured using UV-Vis spectroscopy. The hemolysis rate (%) was calculated using the following formula:

$$\text{Hemolysis percentage (\%)} = \frac{A_{test} - A_{negative}}{A_{postive} - A_{negative}}$$

Where A_{test}, $A_{negative}$, and $A_{positive}$ represent the absorbance of the test group, negative control, and positive control, respectively.

3. Results

3.1. Preparation and characterization of Zr-IR825 nanoparticles

To synthesize the Zr-IR825 coordination nanoparticles, a mild water bath ultrasonic method was employed to treat a mixed solution containing Zr^{4+} ions and IR825 molecules. The Zr^{4+} ions and IR825 molecules self-assembled into nanoparticles through coordination, similar to Fe-HMME coordination nanoparticles [31,32]. Scanning electron microscope (SEM) images show that Zr-IR825 consists of spherical nanoparticles with an average size of approximately 200 nm (Figure 2a). To investigate the elemental composition and oxidation states of Zr-IR825 nanoparticles, X-ray photoelectron spectroscopy (XPS) was used. The XPS survey spectrum (Figure 2b) indicates that, in addition to C, N, and O from the IR825 ligand, the Zr-IR825 nanoparticles also exhibit a prominent Zr 3d characteristic peak. High-resolution XPS spectra further reveal (Figure 2c) that the Zr 3d orbitals show characteristic double peaks at 184.4 eV and 182.0 eV, corresponding to the $3d_{3/2}$ and $3d_{5/2}$ states of Zr^{4+}, respectively [27,33]. Meanwhile, the C 1s spectrum (Figure S1) also shows characteristic peaks of carbon in different chemical environments, providing further evidence for the formation of the coordination structure. Additionally, in the Fourier transform infrared spectroscopy (FTIR) spectrum (Figure 2d), compared to IR825, Zr-IR825 shows the disappearance of the carboxylic acid (C = O) stretching band at 1730 cm^{-1}. Instead, characteristic absorption bands of carboxylate salts appear at 1560 cm^{-1} and 1315 cm^{-1}, indicating that Zr^{4+} has coordinated with the carboxyl groups of IR825 molecules, leading to the formation of the final nanoparticles. The Zeta potential test results showed that the potential of IR825 molecules was −31.9 mV, while after nanoparticle formation, the potential increased to −12 mV. This further confirmed the successful coordination between Zr^{4+} and the IR825 (Figure S2).

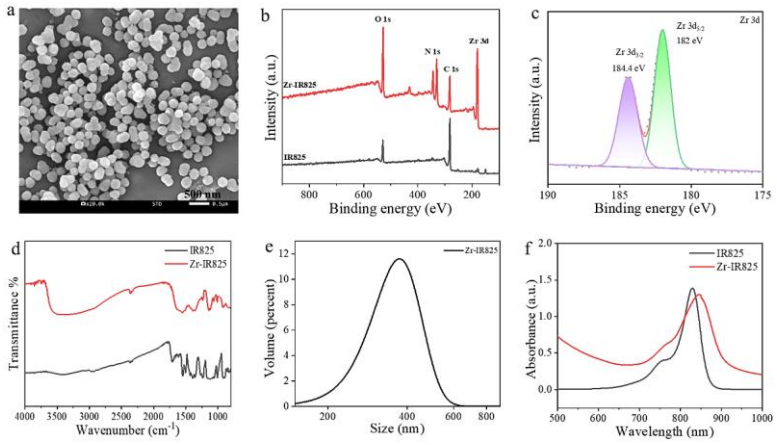

Figure 2. Characterization of Zr-IR825 nanoparticles. **(a)** SEM image of Zr-IR825 nanoparticles; **(b, c)** XPS spectrum and high-resolution Zr 3d spectrum of Zr-IR825 nanoparticles; **(d)** FTIR spectra of Zr-IR825 nanoparticles and IR825 molecules; **(e)** DLS characterization of Zr-IR825 nanoparticles; **(f)** UV absorption spectra of Zr-IR825 nanoparticles and IR825 molecules.

Finally, we investigated the hydrodynamic size and light absorption behavior of Zr-IR825 coordination nanoparticles in solution. DLS data indicate that the average hydrodynamic size of Zr-IR825

nanoparticles is 373.9 nm (Figure 2e), which is an increase of about 123.9 nm compared to the size of the dry Zr-IR825 nanoparticles (as shown in Figure 1a). This increase is likely due to the stretching of the surface ligand PVP in solution [26]. The UV-Vis absorption spectrum (Figure 2f) shows that, compared to free IR825, Zr-IR825 nanoparticles exhibit a broader absorption range in the near-infrared region, which can be attributed to the effect of metal coordination. The Zr-IR825 nanoparticles, with excellent near-infrared light absorption, are expected to have superior photothermal conversion performance, and we will further investigate their photothermal conversion properties in the following sections.

3.2. Photothermal conversion performance study

To investigate the photothermal conversion performance of Zr-IR825 nanoparticles, we first tested the heating behavior of aqueous dispersions of nanoparticles at different concentrations (0–0.4 mg/mL) under 808 nm NIR laser irradiation (0.8 W/cm^2). As shown in Figure 3a, after 5 min of irradiation, the temperature of the 0.1, 0.2, 0.3, and 0.4 mg/mL groups increased by 15.9, 22.1, 27.4, and 35.5 °C, respectively, while the control group (pure water) only increased by 3.3°C. This demonstrates a clear concentration-dependent temperature increase. Infrared thermal images (Figure 3b) further show that the signal intensity of the 0.3 mg/mL group significantly increased with prolonged irradiation time, confirming its excellent photothermal response. Next, we examined the effect of laser power density (0.3–1.0 W/cm^2) on the heating effect at a fixed concentration (0.3 mg/mL). The results indicated that the temperature increased with higher power densities, reaching a maximum temperature rise of 30.2 °C at 1.0 W/cm^2 (Figure 3c). The photothermal conversion efficiency of Zr-IR825 was calculated to be 35.7% based on the heating-cooling curve (Figures 3d and S3), a value significantly higher than that of free IR825 molecules (16.77%) and the FDA-approved ICG (20.56%) (Figure S4). Furthermore, this efficiency is comparable to that of recently reported high-performance inorganic photothermal agents such as CuS@Cu-MOF (39.6%) and Bi_2Se_3 (34.6%) [34,35]. More importantly, after four cycles of laser on-off switching, the nanoparticle still maintained stable heating ability, while ICG showed a significant decrease in temperature rise, indicating good photothermal stability (Figure 3e). These results demonstrated that Zr-IR825 nanoparticles possessed excellent photothermal conversion performance, dual dependence on concentration and power, and cyclic stability, making them an ideal agent for photothermal therapy of tumor cells.

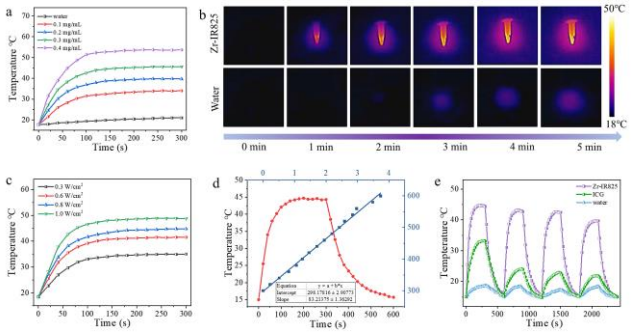

Figure 3. Photothermal conversion properties of Zr-IR825 nanoparticles. **(a, b)** Photothermal heating curves and corresponding thermal images of Zr-IR825 nanoparticles at different concentrations; **(c)** Photothermal heating curves of Zr-IR825 nanoparticles at different laser power densities; **(d)** Heating and cooling curves of Zr-IR825 nanoparticles during laser on/off cycles and the time constant (τs); **(e)** Photothermal stability curves of Zr-IR825 nanoparticles and ICG.

3.3. In vitro cell experiments

Good biocompatibility is essential for the application of materials in *in vitro* tumor therapy. Therefore, we co-incubated Zr-IR825 nanoparticles with 4T1 cells and mouse fibroblast (L929) cells in the dark for 48 hours, and cell viability was measured using the CCK-8 assay. As shown in Figure S5, even at a nanoparticle concentration of 200 μg/mL, the survival rates of both 4T1 and L929 cells remained above 80%, confirming that Zr-IR825 nanoparticles have good biocompatibility and laying the foundation for further tumor treatment studies. To evaluate the *in vitro* photothermal therapeutic effect of Zr-IR825 nanoparticles, 4T1 cells were co-incubated with Zr-IR825 nanoparticles (100 μg/mL) for 6 h. The effect of different laser irradiation times (0–8 min) and laser intensities (0–2 W/cm^2) on cell viability was then studied, and cell viability was assessed using the CCK-8 assay. The results showed that under dark conditions, even at a nanoparticle concentration of 100 μg/mL, the cell viability remained over 99%, indicating that the dark toxicity of Zr-IR825 nanoparticles is negligible. Subsequently, laser irradiation (808 nm, 1.5 W/cm^2) time was extended. As shown in Figure 4a, cell viability decreased as the irradiation time increased. When the irradiation time reached 8 min, cell viability dropped to below 20%. Additionally, Figure 4b demonstrates the effect of different laser intensities on cell viability. Under 0.5 W/cm^2 laser irradiation for 8 min, a slight decrease in cell viability was observed. When the laser intensity increased to 1 W/cm^2, a significant reduction in cell viability was seen, with more than half of the tumor cells dying. At 1.5 W/cm^2, over 80% of the tumor cells were killed. These results suggest that Zr-IR825 nanoparticles can effectively kill tumor cells under near-infrared laser irradiation, and ideal therapeutic outcomes can be achieved by extending the irradiation time or increasing the laser power. To visually demonstrate the *in vitro* photothermal therapeutic effect of Zr-IR825 nanoparticles, the treated cells were stained with Calcein-AM (green fluorescence for live cells) and PI (red fluorescence for dead cells). As shown in Figure 4c, the control group and the Zr-IR825-only group displayed abundant green fluorescence, indicating that the cells remained alive. In the "Zr-IR825 + NIR" group, as the irradiation time increased (from 2 to 8 min), the number of red fluorescence signals gradually increased, while the green fluorescence decreased. At the 6-min and 8-min time points under "Zr-IR825 + NIR" treatment, almost all the visible cells emitted red fluorescence, indicating that a large number of cancer cells had died.

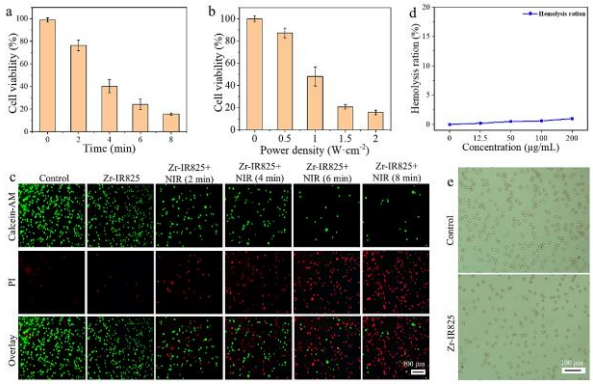

Figure 4. *In vitro* cell experiments with Zr-IR825 nanoparticles. **(a)** Cell viability of 4T1 cells after exposure to Zr-IR825 nanoparticles under different NIR light irradiation times; **(b)** Cell viability of 4T1 cells after exposure to Zr-IR825 nanoparticles under different NIR laser power densities; **(c)** Fluorescence images of 4T1 cells after exposure to Zr-IR825 nanoparticles under different NIR light irradiation times; **(d, e)** Hemolysis rate of red blood cells treated with different concentrations of Zr-IR825 nanoparticles and optical microscope images of red blood cells.

Finally, the biocompatibility of the nanoparticles was evaluated through hemolysis testing. The results showed that even at a Zr-IR825 nanoparticle concentration of 200 μg/mL, the hemolysis rate was well below the 5% threshold set by national standards, indicating that Zr-IR825 nanoparticles are non-hemolytic and exhibit good biocompatibility. Photographs of the mixed solution in a plastic tube (Figure S6) further confirmed this, with the solution remaining clear and no visible hemolysis. Additionally, optical microscopy (Figure 4e) revealed that after incubation with Zr-IR825 nanoparticles (200 μg/mL), red blood cells (RBCs) maintained their typical biconcave disk shape, showing no significant changes compared to the control group. This further demonstrates the excellent biocompatibility of the material.

4. Conclusion

In summary, this study successfully constructed a metal-organic nanoparticle (Zr-IR825) for tumor PTT through a simple and efficient one-step self-assembly strategy. Compared to traditional organic or inorganic nanomaterials used in photothermal therapy, this metal-organic nanoparticle exhibited the following outstanding advantages: (1) Integrated minimalist design: Self-assembly driven by coordination forms a “carrier-free” structure, simplifying the preparation process without the need for a loading step. (2) Excellent photothermal effect: Demonstrating rapid photothermal responsiveness and high photothermal conversion efficiency under NIR laser irradiation, showing significant therapeutic effects *in vitro* photothermal therapy. (3) Good biocompatibility: Exhibiting low cytotoxicity and excellent blood compatibility *in vitro* cell experiments and blood studies. This work not only provided a feasible strategy based on metal-ligand self-assembly for developing efficient, low-toxicity NIR photothermal agents but also offered new insights for expanding the biomedical applications of structurally similar phthalocyanine molecules.

5. Supplementary data

The authors confirm that the supplementary data are available within this article.

Acknowledgments

This work was funded by the Natural Science Foundation of Hubei Province (2024AFB059), the National Natural Science Foundation of China (22171163), the 111 Project of China (D20015) and the Yichang Natural Science Research Program (A23-2-025), the Projects of Scientific and Technological Research of Hubei Provincial Department of Education (Q20241203).

Authors’ contribution

Conceptualization, P.G. and S.X.; methodology, P.G. and Y.H.; software, Y.H., Q.J. and G.F.; validation, P.G., W.H. and S.X.; formal analysis, W.W. and Q.J.; investigation, Y.H., G.F., W.W., S.X., Q.J., W.H. and P.G.; resources, P.G. and S.X.; data curation, Y.H. and G.F.; writing—original draft preparation, S.X. and P.G.; writing—review and editing, P.G.; supervision, P.G. and S.X.; project administration, P.G., W.H. and S.X.; funding acquisition, P.G. and S.X. All authors have read and agreed to the published version of the manuscript.

Conflicts of interests

The authors declare no conflict of interest.

References

[1] Sung H, Ferlay J, Siegel RL, Laversanne M, Soerjomataram I, *et al.* Global cancer statistics 2020: GLOBOCAN estimates of incidence and mortality worldwide for 36 cancers in 185 countries. *CA-Cancer J. Clin.* 2021, 71(3):209–249.

[2] Haidar ZS. Polymicellar-based drug delivery systems for use in nanodentistry, oral and cranio-maxillo-facial oncology. *Biofunct. Mater.*2023, 1(1):0003.

[3] Guo Q, Wang J, Guo J, Wu QY, Li S, *et al.* Biomedical micro/nanomotors: driven mechanism, preparation and physiological barriers breakthrough. *Coord. Chem. Rev.* 2025, 530:216441.

[4] Li Y, Huang L, Li X, Geng P, Xiang J, *et al.* From biomaterials to biotherapy: cuttlefish ink with protoporphyrin IX nanoconjugates for synergistic sonodynamic-photothermal therapy. *J. Mater. Chem. B* 2024, 12:1837–1845.

[5] Wang W, Huang Y, Zhang Y, Xiao S, Luo D, *et al.* Research progress of multifunctional inorganic nanomaterials for tumor photothermal therapy. *Nanoscale* 2025, 17:21938–21960.

[6] Zheng M, Zhang H, Dai M, Yu H, Hu Y, *et al.* A PTT-induced feed-back carbon nanosystem for enhanced breast cancer therapy by extracellular matrix remodeling. *Nano Lett*. 2025, 25(8):3180–3190.

[7] Liu G, Zou J, Tang Q, Yang X, Zhang Y, *et al.* Surface modified Ti_3C_2 MXene nanosheets for tumor targeting photothermal/photodynamic/chemo synergistic therapy. *ACS Appl. Mater. Interfaces* 2017, 9(46):40077–40086.

[8] Wei C, Jin X, Wu C, Brozovic A, Zhang W, *et al.* Carbon spheres with high photothermal conversion efficiency for photothermal therapy of tumor. *Diamond Relat. Mater.* 2022, 126:109049.

[9] Chao Z, Wu K, Sun J, Wang M, Ju H, *et al.* Manipulating ICG J-aggregation and disaggregation for imaging-guided cancer therapy with self-reporting efficiency. *Adv. Healthcare Mater*. 2025, 14:2405032.

[10] Geng P, Xiang G, Zhang W, Lan H, Xiao S, *et al.* Hollow copper sulfide loaded protoporphyrin for photothermal-sonodynamic therapy of cancer cells (In Chinese). *Chinese J. Inorg. Chem*. 2024, 40(10):1903–1910.

[11] Niu S, Geng P, Wang Y, Wen M, Yu N, *et al.* Design and synthesis of multifunctional inorganic nanomaterials for imaging-guided photothermal therapy of tumors. *Adv. Interv. Mater.* 2025, 1(1):100004.

[12] Chen Y, Li L, Chen W, Chen H, Yin J, *et al.* Near-infrared small molecular fluorescent dyes for photothermal therapy (In Chinese). *Chinese Chem. Lett*. 2019, 30:1353–1360.

[13] Zhou B, Li Y, Niu G, Lan M, Jia Q, *et al.* Near-infrared organic dye-based nanoagent for the photothermal therapy of cancer. *ACS Appl. Mater. Interfaces* 2016, 8(44):29899–29905.

[14] Valiveti CK, Kumar B, Singh AD, Biradar SK, Ahmad R, *et al.* Stable dietary ora-curcumin formulation protects from experimental colitis and colorectal cancer. *Cells* 2024, 13(11):957.

[15] Wei Y, Zeng M, Pi C, Shen H, Yuan J, *et al.* Novel curcumin derivative-decorated ultralong-circulating paclitaxel nanoparticles: a novel delivery system with superior anticancer efficacy and safety. *Int. J. Nanomed*. 2022, 17:5265–5286.

[16] Zhu Y, Jia H, Duan Q, Liu X, Yang J, *et al.* Photosensitizer-doped and plasma membrane-responsive liposomes for nuclear drug delivery and multidrug resistance reversa. *ACS Appl. Mater. Interfaces* 2020, 12:36882–36894.

[17] Wang W, Huang Y, Li Y, Geng P, Lan H, *et al.* Multifunctional metal–organic frameworks and their heterojunction materials for cancer theranostics. *Biomater. Sci*. 2025, 13:4081-4096.

[18] Yu F, Wang T, Wang Y, Liu L, Liu T, *et al.* Peroxynitrite-responsive near-infrared fluorescent imaging guided synergistic chemo-photodynamic therapy via biomimetic metal–organic frameworks. *ACS Appl. Mater. Interfaces* 2024, 16:65796–65808.

[19] Li Y, Li Y, Yang J, Wang B, Yin J, *et al.* Ultrasonically assisted self-assembly of multifunctional iron-protoporphyrin nanoparticles and multimodal tumor therapy (In Chinese). *Chem. J. Chinese Universities* 2025, 46:20250176.

[20] Geng P, Li Y, Macharia DK, Ren X, Meng R, *et al.* One stone, three birds: design and synthesis of "all-in-one" nanoscale Mn-porphyrin coordination polymers for magnetic resonance imaging-guided synergistic photodynamic-sonodynamic therapy. *J. Colloid Interface Sci.* 2024, 660:1021–1029.

[21] Hu X, Li R, Wu W, Fang K, Zhu Z, *et al.* A Fe (III)-porphyrin-oxaliplatin (IV) nanoplatform for enhanced ferroptosis and combined therapy. *J. Controlled Release* 2022, 348:660–671.

[22] Liang S, Xiao X, Bai L, Liu B, Yuan M, *et al.* Conferring Ti-based MOFs with defects for enhanced sonodynamic cancer therapy. *Adv. Mater*. 2021, 33:2100333.

[23] Lee J, Yu K, Davaa E, Jenjob R, Tran PH, *et al.* Autophagy-regulating, photothermal polydopamine-coated, and photodynamic zirconium/porphyrin-framed metal–organic frameworks for enhanced doxorubicin therapy in colon cancer. *Biomater. Res*. 2025, 29:0218.

[24] Li C, Yi D, Li M, Li Z. A DNA-MOF hybrid nanosystem for prediction of photodynamic therapy efficacy via amplified imaging of apoptotic mRNA. *Nano Today* 2025, 65:102837.

[25] Wang Z, Sun Q, Liu B, Kuang Y, Gulzar A, *et al.* Recent advances in porphyrin-based MOFs for cancer therapy and diagnosis therapy. *Coord. Chem. Rev*. 2021, 439:213945.

[26] Wang W, Li Y, Li Y, Huang Y, Geng P, *et al.* Titanium-protoporphyrin IX coordinated nanoparticles for tumor photodynamic and sonodynamic combination therapy. *Biofunct. Mater.* 2025, 2:0009.

[27] Li Y, Wang W, Zhang Y, Xiao S, Lan H, *et al.* Design and synthesis of nanoscale Zr-porphyrin IX framework for synergistic photodynamic and sonodynamic therapy of tumors (In Chinese). *Acta Chim. Sin.* 2024, 82(4):443–448.

[28] Sun X, He G, Xiong C, Wang C, Lian X, *et al.* One-pot fabrication of hollow porphyrinic MOF nanoparticles with ultrahigh drug loading toward controlled delivery and synergistic cancer therapy. *ACS Appl. Mater. Interfaces* 2021, 13:3679–3693.

[29] Zhu J, Chu C, Li D, Pang X, Zheng H, *et al.* Fe (III)-porphyrin sonotheranostics: a green triple-regulated ROS generation nanoplatform for enhanced cancer imaging and therapy. *Adv. Funct. Mater.* 2019, 29:1904056.

[30] Wang C, Cao F, Ruan Y, Jia X, Zhen W, *et al.* Specific generation of singlet oxygen through the russell mechanism in hypoxic tumors and GSH depletion by Cu-TCPP nanosheets for cancer therapy. *Angew. Chem. Int. Ed.* 2019, 58:1–6.

[31] Xu H, Yu N, Zhang J, Wang Z, Geng P, *et al.* Biocompatible Fe-hematoporphyrin coordination nanoplatforms with efficient sonodynamic-chemo effect on deep-seated tumors. *Biomaterials* 2020, 257:120239.

[32] Wen M, Shen J, Wang Z, Guo H, Geng P, *et al.* A cascaded enzyme-loaded Fe-hemoporfin framework for synergistic sonodynamic-starvation therapy of tumors. *Nanoscale* 2021, 13:5910–5920.

[33] Ye G, Wan L, Zhang Q, Liu H, Zhou J, *et al.* Boosting catalytic performance of MOF-808(Zr) by direct generation of rich defective Zr nodes via a solvent-free approach. *J. Inorg. Chem.* 2023, 62:4248.

[34] Geng P, Yu N, Macharia DK, Meng R, Qiu P, *et al.* MOF-derived CuS@Cu-MOF nanocomposites for synergistic photothermal-chemodynamic-chemo therapy. *Chem. Eng. J.* 2022, 441:135964.

[35] Xie H, Li Z, Sun Z, Shao J, Yu X, *et al.* Metabolizable ultrathin Bi_2Se_3 nanosheets in imaging-guided photothermal therapy. *Small* 2016, 12(30):4136–4145.